CHARACTERISTICS OF SURFACE INTEGRITY GENERATED BY OBLIQUE MACHINING OF STEEL PARTS

Wit Grzesik

S u m m a r y

In this study the surface integrity produced by oblique turning of a C45 carbon steel was quantified by means of 2D and 3D surface roughness parameters, strain-hardening effects and associated residual stresses. Surfaces were produced by a special straight-edged cutting tool with large inclination angle of 55^0 equipped with carbide cutting tool inserts. It was documented that oblique machining performed with relatively higher feed rate allows to obtain lower surface roughness and, in general, better bearing characteristics. Moreover, compressive stresses with the maximum value located close to the machined surface and with parabolic profile can be induced into the surface layer. The magnitude of stresses depends on the strain-hardening rate of the surface layer.

Keywords: Oblique turning, steel, surface roughness, surface integrity, service properties

**Charakterystyka technologicznej warstwy wierzchniej generowanej
w ukośnym skrawaniu elementów maszyn ze stali**

S t r e s z c z e n i e

W pracy charakteryzowano stan technologicznej warstwy wierzchniej wytworzonej w ukośnym toczeniu stali C45. Stosowano kryteria parametrów chropowatości powierzchni 2D i 3D, efektu umocnienia odkształceniowego i naprężeń własnych. Powierzchnie kształtowano specjalnym narzędziem z węglików spiekanych, w którym prostoliniowa krawędź skrawająca ma duży kąt pochylenia 55^0. Analiza wyników badań pozwala stwierdzić, że ukośne skrawanie prowadzone z dużą wartością posuwu pozwala uzyskać powierzchnię o mniejszej chropowatości i lepszej nośności. Dodatkowo w warstwie wierzchniej są wytworzone ściskające naprężenia własne o maksymalnej wartości w pobliżu powierzchni i profilu parabolicznym. Wartość maksymalna naprężeń ściskających zależy od stopnia umocnienia odkształceniowego materiału warstwy wierzchniej.

Słowa kluczowe: toczenie ukośne, stal, właściwości warstwy wierzchniej, właściwości użytkowe

1. Introduction

It is obviously known that oblique machining processes dominate in practical metal cutting operations, such as turning, drilling, milling, broaching

Address: Prof. Wit GRZESIK, Opole University of Technology, Faculty of Mechanical Engineering, ul. Mikołajczyka 5, 45-271 Opole, Phone: (+48, 77) 4006290, Fax: (+48, 77) 4006342, e-mail: w.grzesik@po.opole.pl

and hobbing. From this point of view, the knowledge about the oblique machining process seems to be of considerable interest to the manufacturing industry. The majority of practical cutting tools have oblique non-straight cutting edges [1] and values of the inclination angle range from several (for example turning tools) to dozens degrees (for example milling cutters) [2]. Several positive effects can be observed under such machining conditions, including: the reduction of the undeformed chip thickness, the formation of the subsurface layer with large negative rake angles, lower cutting force and the production of the machined surface with a lower surface roughness at higher feed rates [3]. On the other hand, higher radial forces produced by tools with large inclination angles can result in the generation of chatter on insufficiently stiff machine tools which degrades surface finish.

Oblique machining is performed under specific machining conditions, including very large negative working angle and extremely small minimum undeformed chip thickness, which results in a severe plastic deformation of the surface layer, which is distinctly stronger than in conventional machining processes with nose-rounded tools. It should then be aimed for compressive residual stresses to be induced into the technologically modified surface layer.

The emphasis of this paper is laid on the facilitation of the design of turning tools involved particularly in the precision machining of cylindrical surfaces and the consequent improvement of the productivity of this process.

It should be noticed that a straight cutting edge is the simplest geometry for material removal and it is less costly in comparison to complex, sometimes very sophisticated, geometries of the commercial cutting tool inserts.

Optionally, it is possible to use straight edges of cutting tool inserts between worn corners, which prolongs their durability and reduces the tool costs. In practice, surface roughness depends considerably, when using tools with geometrically defined cutting edges, on such factors as geometry of the cutting wedge, cutting parameters, as well as grade, microstructure and mechanical properties of the machined work material [4].

In this paper, a very detailed analysis of the machined surface and the surface layer was performed for steel and spheroidal iron parts generated by carbide and mixed ceramic tools with highly inclined cutting tool edges. Moreover, the effects of oblique turning operations were examined not only on the parts made of popular steel grades and spheroidal iron with different mechanical properties and microstructures but also on hardened steel parts.

2. Characteristics of slant tools for oblique machining

In this study oblique machining is represented by external cylindrical turning using a straight-edged (slant) tool with a large inclination angle as shown in Fig. 1. This special case of turning was termed "free oblique turning". It is

obviously known that, based on the kinematic model of the conventional cutting process, the shape of an individual cutting edge trace, which constitutes the surface profile or surface topography, is a function of the feed rate f and the tool corner radius r_ε [5]. On the other hand, in the case of a straight-edged oblique tool for which this radius is equal to infinity, it is possible to introduce an equivalent tool with the corner radius equal to the curvature of hyperbola r_{eq} (axial cross-section of the hyperboloid) shown in Fig. 1b.

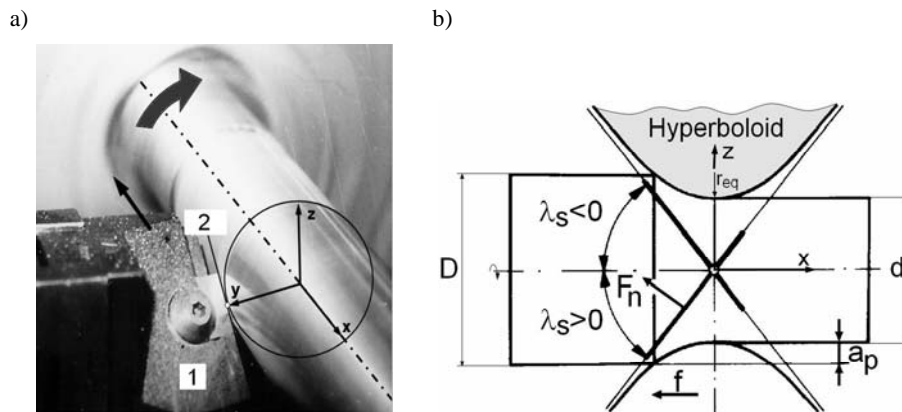a)   b)

Fig. 1. Free oblique turning using straight-edged tool: a) general view, b) scheme showing the sign of inclination angle and the formation of the machined surface; 1 – slant tool, 2 – inclined straight cutting edge, F_n – normal force, D – diameter of the workpiece, d – diameter of the machined surface, a_p – depth of cut

According to the scheme shown in Fig. 1b, the surface roughness results from the unremoved material between the rotary hyperboloids formed during two subsequent rotations of the workpiece. Its theoretical height can be determined as follows [3]:

$$Rzt = \sqrt{\left(\frac{D}{2} - a_p\right)^2 + \frac{f^2\tan^2\lambda_{sf}}{4\sin^2\lambda_{sp}}} - \left(\frac{D}{2} - a_p\right) \tag{1}$$

where D is the diameter of the workpiece in mm, f is the feed rate in mm/rev, a_p is the depth of cut in mm, λ_{sf} and λ_{sp} are projections of the inclination angle λ_s on the assumed working P_f and tool back P_p planes respectively, shown in Fig. 2.

When the angle λ_{sp} is equal to 90^0 ($\lambda_{sf} = \lambda_s$, $\kappa_r = 0$) and $a_p \ll D$, Eq. (1) can be simplified as [6]:

$$Rzt = \frac{D}{2}\left(\sqrt{\left(\frac{f}{D}\right)^2 \tan^2\lambda_s + 1} - 1\right) \tag{2}$$

The radius of the curvature of hyperbola r_{eq} denoted in Fig. 1b can be expressed as

$$r_{eq} = \frac{(D - a_p)\cos^2\kappa_r}{2(\tan^2\lambda_s + \sin^2\kappa_r)} \quad \text{or} \quad r_{eq} = \frac{D - a_p}{2\tan^2\lambda_s} \quad \text{for} \quad \kappa_r = 0 \tag{3}$$
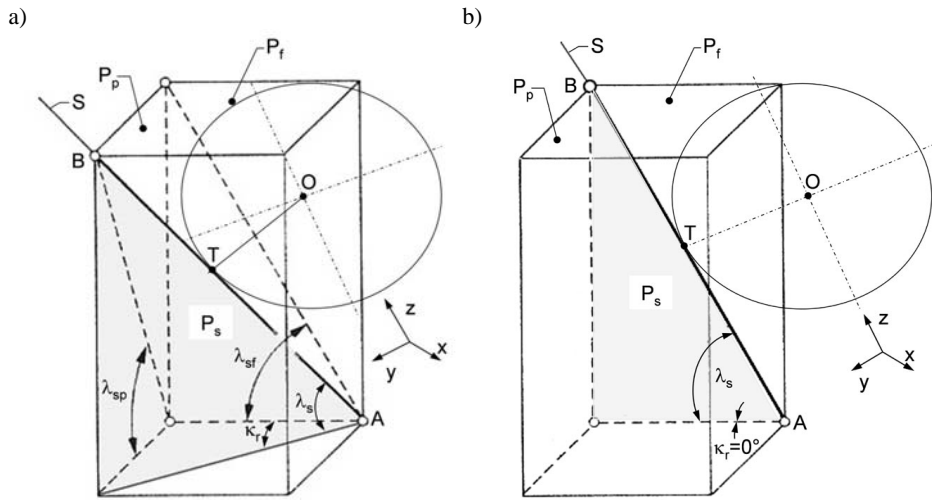
a) b)

Fig. 2. Scheme showing the localization of the cutting edge versus workpiece: a) case when $\lambda_{sp} < 90^0$ and $\kappa_r > 0$, b) case when $\lambda_{sp} = 90^0$ and $\kappa_r = 0$; T – tangential point, O – workpiece axis

For the diameter of the workpiece and cutting conditions used, the calculated values of Rzt are about 0.3 μm and 0.45 μm for the feed rates of 0.17 and 0.21 mm/rev respectively. The curvature radius r_{eq} calculated from Eq. 3 is equal to about 12.30 mm.

3. Performance of the experiment

3.1. Workpiece material, cutting tools and machining conditions

Machining trials were performed on the specimens made of C45 carbon steel in normalized state. Chemical compositions of the selected materials and

their mechanical properties are specified in Tables 1 and 2 respectively. The bars made of carbon steel were machined with uncoated P20 carbide tools.

All cutting conditions employed for the turning operations performed, and characteristics of the tools used are specified in Table 3.

Table 1. Chemical compositions of workpiece material machined

Steel grade	Microstructure	Chemical composition, %					
		C	Mn	Si	Cr	Ni	S
C45	Pearlite + Ferrite	0.45	0.65	0.25	0.20	0.20	0.04

Table 2. Mechanical properties of workpiece material

Steel grade	Ultimate tensile strength Rm, MPa	Yield strength Re, MPa	Elongation A_5, %	Hardness HB
C45	670	420	16	240

Table 3. Specifications of machining conditions

Workpiece material	Machining operation	Cutting parameters
C45	Turning with P20 uncoated carbide tool, $\lambda_s = 55°$, $\gamma_n = -15^0$, $\alpha_n = 10^0$	$v_c = 70\text{-}280$ m/min, $f = 0.08\text{-}0.54$ mm/rev, $a_p = 0.25$ mm

3.2. Measurements of surface roughness

In this study a TOPO-01P profilometer with a diamond stylus radius of 2 μm was used to measure 2D and 3D roughness parameters. The roughness parameters were estimated on the scanned areas of 2.4 mm × 2.4 mm. The sampling displacements were chosen to be $\Delta x = 0.5$ μm and $\Delta y = 12.4$ μm respectively. 3D roughness parameters were determined as the average values captured on 4 elementary areas of 0.8 mm × 0.8 mm. On the other hand, 2D roughness parameters were estimated on the surface profile containing 3 elements of 0.8 mm length each, and the arithmetic average results were calculated taking into account about 200 surface profiles generated.

3.3. Measurements of physical properties of surface layer

In the second part of the experimental work some important properties of the surface layer were measured, including the distribution of HV hardness beneath the surface, strain-hardening effect and its depth, as well as the maximum compressive stresses and their localization. Moreover, the thickness

of the hardened and stressed zones was assessed based on the hardness distribution and residual stress profile.

Micro-hardness (μHV) across the surface layer was measured using the Vickers hardness tester at the load of 1 N i.e. $HV_{0.1}$. Hardness variation within subsurface layer of about 50 μm thickness was determined. In order to avoid interference of indentations and increase the measuring accuracy, the measurements were performed on the oblique sections, inclined at about 3° to the outer surface. Based on the hardness data, the strain-hardening rates in the measuring points were computed in comparison to the bulk material with initial mechanical properties.

The maximum value of the strain hardening rate (*SHR*) was determined as

$$SHR = \frac{HV_{max} - HV_{bm}}{HV_{bm}} \tag{4}$$

where HV_{max} is the maximum hardness in the vicinity of the machined surface and HV_{bm} is the hardness of the bulk material.

Residual stresses induced in the surface layer were measured using the destructive method in which the outer layer of a slotted ring was continuously etched of by means of a 3% vol. water solution of nitride acid (HNO_3). Due to the relaxation effect, the ring deforms and the deformations (f_i) corresponding to the thicknesses of etched layers (a_i) are recorded. Consequently, after the derivation of the *f-a* curve the circumferential (tangential) residual stresses can be determined.

All the above-mentioned characteristics of the surface layer were investigated in terms of two independent variables, including the cutting speed (x_1), the feed rate (x_2), keeping constant the depth of cut, the normal rake angle and the normal clearance angle. Capital letters denote logarithmic values of process variables. As a result, several multi-regressive polynomial models in the form of exponential models for natural variables (Eq. 3.2) are provided.

$$y = x_o^{k_0} \times x_1^{k_1} \times x_2^{k_2} \tag{5}$$

The mathematical model expressed by Eqn. 3.2 was successively applied to predict the surface roughness Ra, the strain hardening rate (*SHR*), the depth of strain-hardened layer (h_{SH}), the maximum residual stress (σ_{cmax}) and the depth of stressed layer (h_{STR}). The experimentally obtained values of SL characteristics and corresponding mathematical models are presented in Section 4.

4. Experimental results and discussion

4.1. Surfaces produced by oblique turning

As mentioned above in Section 3, the surface integrity produced by oblique turning with straight cutting edge was characterized by means of 2D and 3D surface roughness, bearing characteristics, surface texture (lays), distribution of microhardness, and residual stresses induced in the subsurface layer. In the second part of this section, the properties of the generated SL are predicted based on the mathematical models overviewed in Section 3.3.

In particular, the surface roughness produced on the machined parts was characterized by 4 groups of ISO surface roughness parameters (height, spacing, hybrid and material/amplitude distribution), as proposed by ISO Standards [7]. A set of values of both 2D and 3D roughness parameters is selected in Table 4. Figure 3 presents the surface topography and contour map visualized by means of a Surfer v.9 software, generated by the straight-edged tool using high cutting speed of 280 m/min and medium feed rate of 0.17 mm/rev. Moreover, Fig. 4 illustrates characteristic surface texture and the shape of surface profile. For these cutting conditions the Ra and Rz roughness parameters are equal to 0.8 μm
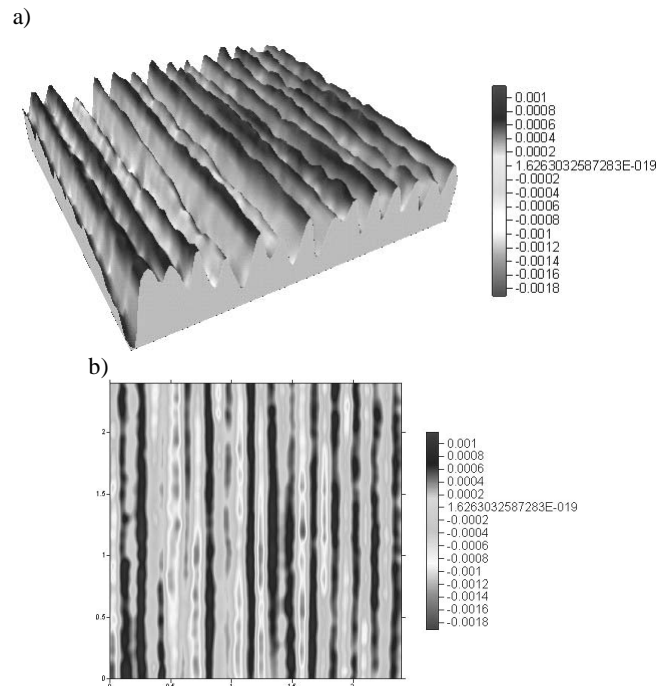

Fig. 3. Filtered surface topography (a) and contour map (b) generated using Surfer v.9 software. Cutting conditions: $v_c = 280$ m/min, $f = 0{,}17$ mm/rev, $a_p = 0{,}25$ mm
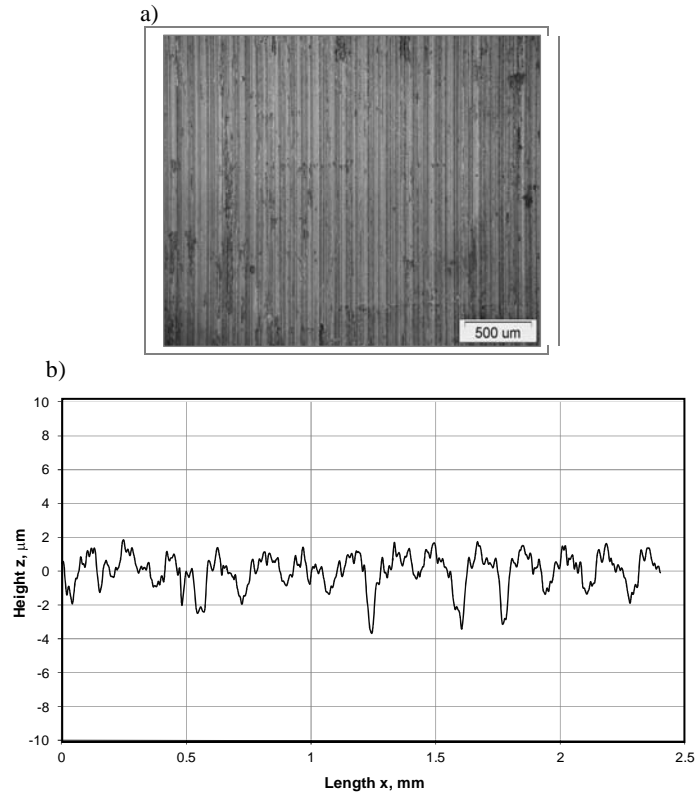
a)

b)

Fig. 4. Surface LOM image showing characteristic lays at magnification 50× (a) and recorded
surface profile (b). Cutting parameters: v_c = 280 m/min, f = 0.17 mm/rev, a_p = 0.25 mm
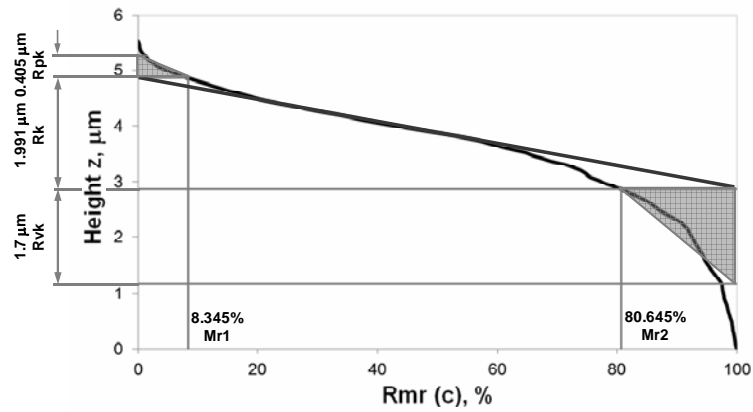

Fig. 5. Bearing area curve after oblique machining for C45 steel. Cutting conditions:
v_c = 280 m/min, f = 0.17 mm/rev, a_p = 0.25 mm

and 4.7 µm respectively. It should be noted that the generated surface is distinguished by the negative skewness of about -1, which suggests acceptable bearing properties. More detailed description of the BAC is presented in Fig. 5.

For the bearing curve shown in Fig. 5, the bearing area parameters are: $Rk = 2.0$ µm, $Rpk = 0.40$ µm, $Rvk = 1.70$ µm, MR1 = 8.345%, MR2 = 80.645%. In particular, the reduced peak height is very small ($Rpk = 0.40$ µm), so the part of the machined surface being removed during running-in period is also very small.

Among 3D roughness parameters a group of volume and area parameters is particularly important, including the Vm (material volume of the surface), the core void volume (Vvc) and the valley void volume (Vvv) parameters, which are based on the 3D BAC and termed "*volume*" functional parameters. For the case study presented in this section their values are equal to $Vm = 1.1 \times 10^4$ µm^3/mm^2, $Vvc = 68 \times 10^4$ µm^3/mm^2 and $Vvv = 2.13 \times 10^4$ µm^3/mm^2 respectively.

4.2. Prediction of SL characteristics

Based on the mathematical models derived using Eqn. (3.2) its graphical representations in the form of the response surfaces are presented successively in Figs. 6-8. Fig. 6 presents the response surface $Ra = f(v_c, f)$ described by Eqn. 6.
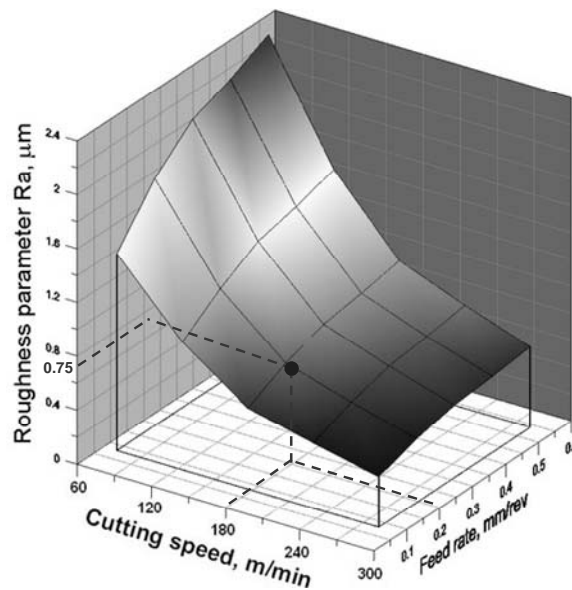

Fig. 6. The influence of cutting speed and feed rate on the roughness parameter Ra.
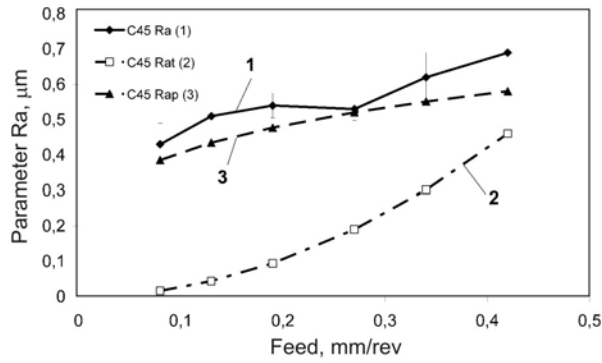Cutting conditions: $a_p = 0.50$ mm, $\gamma_n = -15°$, $\alpha_n = 10°$

Fig. 7. The influence of feed rate on the roughness parameter *Ra*.
Cutting conditions: $vc = 280$ m/min, $a_p = 0.50$ mm, $\gamma_n = -15°$, $\alpha_n = 10°$

The relevant model describing the response surface Ra = f(v_c,f) is shown in
Fig. 6, keeping $a_p = 0.50$ mm, $\gamma_n = -15°$, $\alpha_n=10°$is

$$Rap = 184.7302 \times v_c^{-0.9845} \times f^{0.2474} \tag{6}$$

In order to compare the measured values of the *Ra* parameter with both
predicted (Rap) values using Eqn. (6) and theoretical ($Rat = f^2/8r_{eq}$) values using
Eqn. (3), Fig. 7 shows how they change when feed rate increases. It can be noted
that theoretical *Rat* values differ substantially from the measured and predicted
data similarly to conventional cutting with defined corner radius [4-6].

The relevant models describing the response surfaces corresponding to the
strain-hardening and its depth beneath the machined surface, shown in Figs. 8 a
and b, keeping $a_p = 0.50$ mm, $\gamma_n = -15°$, $\alpha_n=10°$are

$$SHR = 364.3595 \times v_c^{-0.3894} \times f^{0.6064} \tag{7a}$$

$$h_{SH} = 169.9052 \times v_c^{-0.2103} \times f^{0.3134} \text{ in μm} \tag{7b}$$

It can be seen in Fig. 8a that the surface layer is mostly hardened at the
lowest cutting speed and the highest feed applied and in this case $SHR \approx 50\%$
and $h_{SH} \approx 60$ μm. On the contrary, the lowest strain hardening is associated with
the highest cutting speed and the lowest feed ($SHR \approx 10\%$ and $h_{SH} \approx 25$ μm). The
depth of strain-hardened layer, as the response function of the cutting speed and
feed rate, is shown in Fig. 8b.

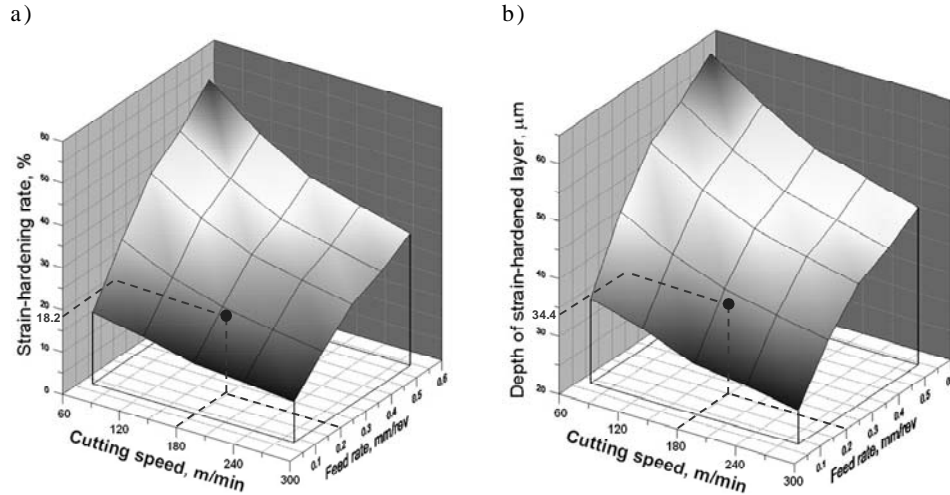a)   b)

Fig. 8. The influence of cutting speed and feed rate on the strain-hardening rate (a) and the depth of strain-hardened layer. Cutting conditions: $a_p = 0.50$ mm, $\gamma_n = -15°$, $\alpha_n = 10°$

It can be seen from Fig. 8b that plastic deformation penetrates deeply when using lower cutting speeds and higher feed rates. For such a combination of cutting parameters the maximum depth of strain-hardened layer approaches 60 μm.

The relevant models describing the response surfaces corresponding the maximum values of residual stresses and their localization shown in Figs. 9a and b, keeping $a_p = 0.50$ mm, $\gamma_n = -15°$, $\alpha_n = 10°$ are

$$\sigma_{c\max} = 288.4024 \times v_c^{-0.0841} \times f^{0.4097}$$

(8a)

$$h_{STR} = 342.9937 \times v_c^{-0.3743} \times f^{0.2978} \qquad (8b)$$

For instance, the predicted values of surface layer characteristics, keeping $v_c = 180$ m/min, $f = 0.20$ mm/rev and $a_p = 0.5$ mm are: $Ra = 0.75$ μm, $SHR = 18.2\%$, $h_{SH} = 34.4$ μm, $\sigma_{cmax} = -96.4$ MPa, $h_{STR} = 30.4$ μm. All these values are placed on the relevant response surfaces shown in Figs. 6, 7 and 8, respectively.

It can be observed in Fig. 9 that the generation of residual compressive stresses is strongly associated with the strain-hardening effect, i.e. the cold (mechanical) model of stress generation predominates in the oblique machining [4]. This is due to the fact that the very thin layer of about 3 μm being removed

is plastically deformed to the extreme degree by the cutting edge with a very large negative working rake angle [3, 8]. For instance, for $\lambda_s = 55°$ and $\gamma_n = -15°$, the working rake angle $\gamma_{ne} \approx -35°$, and the shear strain $\gamma_{sh} \approx 12$. As a result, the maximum compressive stresses of about –160 MPa appear when machining with the lowest cutting speed and the maximum feed rate. Moreover, the point of – 96.4 MPa corresponding to the stress distribution is marked in Fig. 9a.

a)   b)
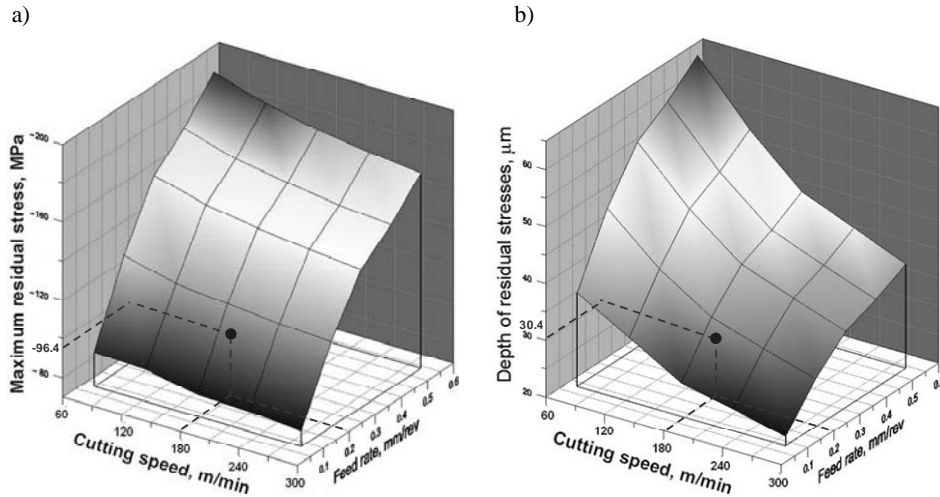

Fig. 9. The influence of cutting speed and feed rate on the maximum residual stress (a) and the depth of stressed layer (b). Cutting conditions: $a_p = 0.5$ mm, $\gamma_n = -15°$, $\alpha_n = 10°$

For such a combination of cutting parameters, the stressed layer penetrates up to about 60 μm (the highest point on the response surface in Fig. 9b). This means that the width of the surface layer can be accurately assessed based on hardness measurements or etching of the stressed layer.

Fig. 10 shows exemplary LOM micrograph and BSD image showing plastic deformations within the pearlitic-ferritic microstructure of C45 carbon steel. The thickness of the surface layer is about 40 μm, which roughly coincides with the measured microhardness profile. Moreover, the zone of extremely intensive plastic deformation of grains, which penetrates about 5 μm beneath the surface can be easily observed in Fig. 10b. This observation underlines the presence of heavy plastic deformations generated by the oblique turning process with a tool having large negative rake angle. In particular, some parts of pearlite grains adjacent to the surface are elongated in the direction of the cutting movement.
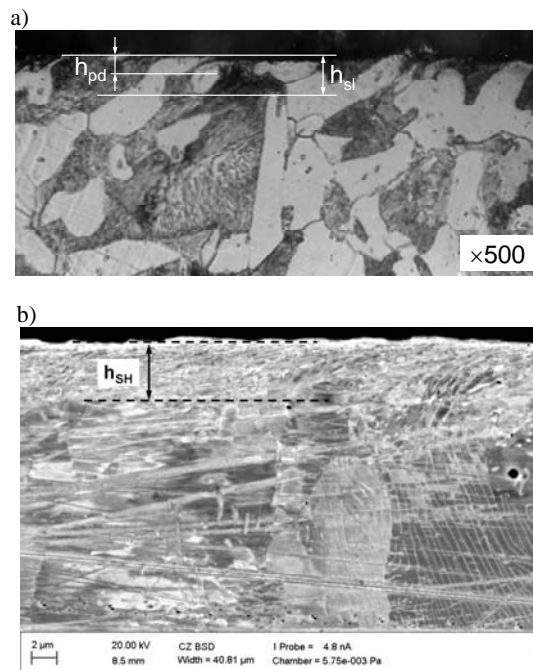
a)

b)

Fig. 10. Micrograph (a) and BSD image (b) showing plastic deformation in the surface layer. Workpiece material – C45 steel. Symbols: h_{sl} – thickness of surface layer, h_{pd} – depth of intensive plastic deformations. Cutting conditions: $v_c = 245$ m/min, $f = 0.34$ mm/rev, $a_p = 0.5$ mm, $\gamma_n = -20°$, $\alpha_n = 10°$

5. Conclusions

The main following conclusions and practical findings resulting from this study are:

• The obtained results highlight the capabilities of oblique turning process as an alternative to conventional finish turning, and even grinding operations demanded in the production of high-quality parts.

• Machining with slant tools can improve surface finish and bearing properties of surfaces on both steel parts. Oblique turning produces surfaces with blunt irregularities which are characterized by the RMS slope ($R\Delta q$) of about 5°.

• In general, oblique turning processes produce Rsk/Rku envelopes, which allow selecting the desired process conditions in order to produce surfaces with desired bearing properties. Moreover, the values of the reduced peak height Rpk of 0.3-0.4 μm were obtained for steel parts.

• Oblique cutting can result in the generation of compressive residual stresses with the maximum value localized close to the machined surface. Their magnitudes depend on the strain-hardening effect and their maximum values approach –200 MPa. In addition, they are accompanied by severe plastic deformations localized near the machined surface.

References

[1] G.P. ZOU, I. YELLOWLEY, R.J. SEETHALER: A new approach to the modeling of oblique cutting process. *Int. J. Mach. Tools Manuf.*, **49**(2009), 701-707.
[2] T.J. DROZDA, CH. WICK: Tool and manufacturing engineers handbook. Vol. I, Machining. SME Technical Divisions, Dearborn 1983.
[3] W. GRZESIK: Stereometric and kinematic problems occurring during cutting with single-edged tools. *Int. J. Mach. Tools Manuf.*, **26**(1986), 443-457.
[4] W. GRZESIK: Advanced machining processes of metallic materials. Elsevier, Amsterdam 2008.
[5] G. BOOTHROYD, W.A. KNIGHT: Fundamentals of machining and machine tools. CRC Press, Boca Raton 2006.
[6] E. MIKO: Constituting micro-irregularities on metallic surfaces using cutting tools with geometrically-defined stereometries (in Polish). Technical University of Kielce, Kielce 2004.
[7] B. GRIFFITHS: Manufacturing surface technology. Penton Press, London 2001.
[8] W. GRZESIK, K. ŻAK: Investigations of surface textures produced by oblique machining of different workpiece materials. *Archives of Materials Science and Engineering*, **52**(2011), 46-53.